Available online at www.sciencedirect.com
SCIENCE DIRECT®
Journal of Molecular Spectroscopy 219 (2003) 45–57
Journal of MOLECULAR SPECTROSCOPY
www.elsevier.com/locate/jms

High resolution absorption cross-section measurements of the Schumann–Runge bands of O_2 by VUV Fourier transform spectroscopy

T. Matsui,[a,1] A.S.-C. Cheung,[b] K.W.-S. Leung,[b] K. Yoshino,[c,*] W.H. Parkinson,[c] A.P. Thorne,[d] J.E. Murray,[d] K. Ito,[e] and T. Imajo[f]

[a] *Tsukuba University, Tsukuba 1-1-1, 305-8573, Japan*
[b] *The University of Hong Kong, Hong Kong*
[c] *Harvard-Smithsonian Center for Astrophysics, 60 Garden Street, Cambridge, MA 02138, USA*
[d] *Blackett Laboratory, Imperial College of Science, Technology, and Medicine, London SW7-2BZ, UK*
[e] *Photon Factory, KEK, Oho, Tsukuba, Ibaraki 305-0801, Japan*
[f] *Japan Women's University, Tokyo 112-8681, Japan*

Received 10 September 2002; in revised form 16 December 2002

Abstract

The photoabsorption spectrum of the O_2 Schumann–Runge bands was measured with resolution comparable to the Doppler widths by using the VUV Fourier transform spectrometer from Imperial College, London, combined with synchrotron radiation as a continuum light source at the Photon Factory, KEK, Japan. The analysis of the (12,0)–(17,0) bands of the Schumann–Runge system provides accurate rotational line positions as well as the line intensities from 185 to 175 nm. Molecular constants of the $v' = 12$ to 17 levels of the $B^3\Sigma_u^-$ state have been determined. The $(v', 0)$ band oscillator strengths were determined as 2.38, 2.62, 2.70, 2.66, 2.40, and 2.12×10^{-5} for the bands from $v' = 12$ to 17, respectively.

1. Introduction

The Schumann–Runge (S–R) band system, which can be found in the photoabsorption spectrum of O_2 in the wavelength region 175–205 nm, is ascribed to the transition from the ground state $X^3\Sigma_g^-$ to the excited state $B^3\Sigma_u^-$. The S–R bands contain many relatively narrow (0.2–4 cm^{-1}) rotational lines belonging to 14 branches (6 principal, 6 satellite, and 2 forbidden branches) of this triplet–triplet transition. Although the upper state $B^3\Sigma_u^-$ is a bound state, it is dissociated by interaction with repulsive states to produce two oxygen atoms in the ground state [1]. This predissociation is the major source of oxygen atoms in the stratosphere (height of 11–48 km) and especially in the mesosphere (height of 48–90 km). Because atomic oxygen plays an important role in the photochemistry of these atmospheric regions, it is necessary to obtain the wavelengths, the oscillator strengths and the linewidths of rovibrational lines in the S–R band for atmospheric photochemical modeling [2].

Spectroscopic aspects of the S–R bands have been extensively reviewed by Krupenie [3], Creek and Nicholls [4], and Huber and Herzberg [5]. The analyses of the S–R bands were initiated by Curray and Herzberg [6], Knauss and Ballard [7], and Brix and Herzberg [8]. Yoshino et al. [9] reviewed and presented the vibronic assignments of the S–R bands. The molecular constants of the $B^3\Sigma_u^-$ state were determined from the experimental data [9] by Cheung et al. [10]. Recently the rotational perturbations in the $B^3\Sigma_u^-$ state were studied by high resolution laser absorption spectroscopy for the (16,0)–(18,0) bands by Lewis et al. [11]. The same group extended the assignments of the S–R bands up to $v' = 22$ [12].

* Corresponding author.
E-mail address: kyoshino@cfa.harvard.edu (K. Yoshino).
[1] Present address: National Institute of Advanced Industrial Science and Technology, Ibaraki 305-8565, Japan.

0022-2852/03/$ - see front matter © 2003 Elsevier Science (USA). All rights reserved.
doi:10.1016/S0022-2852(03)00009-2

Earlier, Bethke determined the band oscillator strengths of the S–R bands by lower resolution photoelectric measurements using the technique of pressure broadening [13]. In 1975, Huebner et al. also determined band oscillator strengths by electron energy loss measurements [14]. More recent determinations of the band oscillator strengths of the S–R bands were made by Frederick and Hudson [15] and Lewis and co-workers [16–20]. The Harvard-Smithsonian Center for Astrophysics (CfA) group measured absorption cross-sections for the (1,0) through (12,0) S–R bands at 300 K [21,22] and 79 K [23] with a resolution of $\simeq 0.40\,\mathrm{cm}^{-1}$ and determined the band oscillator strengths for these bands directly from the measured cross-sections.

In the present paper, we report experimental cross-section data at 295 K throughout the wavelength region 175–182.5 nm containing the $(v',0)$ bands from $v'=12$ to the dissociation limit. The linewidths in the S–R bands above $v'=12$ suddenly become narrower, especially in the (13,0) and the (14,0) bands. Almost all linewidths observed at room temperature for the vibrational bands above $v'=12$ are less than $0.4\,\mathrm{cm}^{-1}$. The highest resolution of conventional spectrometers using gratings is about $0.4\,\mathrm{cm}^{-1}$ in the S–R wavelength region. Therefore, as discussed by Stark et al. [24], it is difficult to obtain precise oscillator strengths of the rovibrational lines of the bands for $v'>12$ with a conventional spectrometer. For this reason we used a new method for the measurement of these bands: Fourier transform (FT) spectroscopy, with synchrotron radiation as a background light source.

Although FT spectroscopy is generally regarded as a technique for the infrared, where the multiplex advantage can be exploited, the FT spectrometer at Imperial College London (IC) is designed for the ultraviolet and operates from the visible region to 140 nm with a resolution limit down to $0.03\,\mathrm{cm}^{-1}$ [25,26]. Using this instrument and a White cell, Yoshino et al. measured the absorption cross-sections of the Herzberg I, II, and III bands of O_2 at a resolution of $0.06\,\mathrm{cm}^{-1}$ (resolving power 750 000) (e.g. [27,28]). However, in order to obtain good signal-to-noise (S/N) ratios in an absorption spectrum in the VUV, it is necessary to use a background continuum source of high photon flux in that region, preferably in conjunction with a predisperser to limit the spectral bandwidth. We therefore moved the FT spectrometer to the Photon Factory synchrotron source in Japan.

2. Experimental

The present experiment was carried out at the Photon Factory (PF), High Energy Accelerator Research Organization (KEK), Japan. PF synchrotron radiation is provided by the storage ring (2.5 GeV). Full details of the experimental setup were described in a previous paper [29]. The FT spectrometer was connected to beam line 12B [30,31] in PF. Synchrotron radiation from the predisperser system in the beam line was reflected by a cylindrical mirror and focused onto the entrance aperture of the FT spectrometer. To ensure full coverage from the (12,0) band to the dissociation limits of O_2, the predisperser was set to produce center wavelengths of 177.5 and 180.0 nm, with a bandwidth of 2.5 nm. The diameter of the entrance aperture was set at 1.5 mm. The spectral resolution was either 0.06 or $0.12\,\mathrm{cm}^{-1}$ by using the maximum optical path difference for the scan of 8.33 or 4.16 cm, respectively. The absorption cell, with an optical path length of 7.82 cm, was placed between the predisperser and the FT spectrometer, and O_2 gas was introduced at pressures of 2.00, 4.00, and 10.00 Torr at room temperature (295 K), corresponding to column densities of 0.51, 1.02, and $2.56\times10^{18}\,\mathrm{cm}^{-2}$. The O_2 pressure was measured with a capacitance manometer (MKS Baratron). For the measurements at $0.12\,\mathrm{cm}^{-1}$ resolution, a total integration time of about 20 h, obtained from around 400 coadded scans, yielded S/N ratios in the continuum background of about 100. The S/N ratios for the spectra observed with a resolution of $0.06\,\mathrm{cm}^{-1}$ were about 50 or less.

3. Analysis of the spectrum

3.1. Fitting of the FT data

The measured absorption spectra were converted to optical depth by taking the logarithms of the intensity (I) and fitting a smooth continuum to the regions between the lines (I_0). The absorption lines were fitted to Voigt profiles using the spectral reduction routine *GREMLIN* [32]. Line parameters (position, width, intensity, and Gaussian and Lorentzian contributions to the Voigt profile) are determined through a nonlinear least-squares iterative procedure. The spectra used for the analysis have a S/N ratio for I_0 of about 100. There are many seriously blended lines in the Schumann–Runge spectrum, particularly the low rotational R_2, R_3 and P_2, P_3 lines for $N=3$ to 11. These blended lines could be separated by taking care to keep the combination rule of line positions for blended $R_{2,3}(N)$ and $P_{2,3}(N+2)$ lines, and to constrain the intensity ratios between these R and P lines to be almost the same, according to the calculated Hönl-London factors discussed by Tatum and Watson [33]. We obtained temporary line parameters from the first fitting results and determined provisional line positions for $R_{2,3}(N)$ and $P_{2,3}(N+2)$ and then we refitted the lines with these new positions. If the line strengths obtained in the second fitting were satisfactory, the line positions should be correct; otherwise the line positions were further

adjusted until the relative line strengths were in good agreement with the intensity ratio estimated from the Hönl-London factors. This procedure is also effective to deconvolute blends between lines in different branches.

The Lorentzian component of the Voigt profile is due to the predissociation of the $B^3\Sigma_u^-$ state, and the Gaussian component is due to Doppler broadening, with a full-width at half maximum (FWHM) of $0.12\,\mathrm{cm}^{-1}$. The instrumental function of the spectrometer can be approximated by a Gaussian function of width $0.12\,\mathrm{cm}^{-1}$, and the convolution of this with the Doppler width should give an effective Gaussian width of $0.17\,\mathrm{cm}^{-1}$. However, the best fit Gaussian component is significantly wider than this, ranging from 0.26 to $0.30\,\mathrm{cm}^{-1}$. These anomalous Gaussian widths are considered to be due to drifts in alignment causing very small wave number shifts over the long observation periods [34]. In our fitting procedure, the Gaussian contribution for each spectrum is kept constant for all lines at the mean value found for that spectrum (i.e., between 0.26 and $0.30\,\mathrm{cm}^{-1}$).

3.2. Line positions and molecular constants

Fig. 1a shows the spectrum of the Schumann–Runge $(v',0)$ bands in the region from 55 450 to 57 500 cm^{-1}, in which the bands for $v'=12$ to 17 are included. We assigned about 650 lines in the present analysis according to the results of Yoshino et al. [9]. An expanded portion of the (14,0) band spectrum is shown in Fig. 1b with details of the rotational structure, which includes the high J lines of the (15,0) and (16,0) bands. The line positions for the (12,0)–(17,0) bands of the S–R system were obtained by averaging over the lines with different experimental conditions. The results are presented in Tables 1a and 1b for the six principal branches and for the satellite and forbidden branches, respectively. About one-fourth of all assigned lines are blended with other lines. In general, the P_1 and R_1 lines are well separated from the $P_{2,3}$ and $R_{2,3}$ lines. However, some of them are blended closely with lines from other bands, for example $R_1(3)$ of the (15,0) band with $R_2(13)$ of the (16,0) band. In Tables 1a and 1b, the partly resolved complexes are labeled with "b." Several high J lines are entirely blended with other strong lines and could not be deconvoluted by the least-square fitting. Such blended lines are analyzed as a single line. Table 1a presents also calculated wavenumbers for the blended high J lines in *italic*, which are derived from the term values.

The perturbation in the (16,0) band, observed by Brix and Herzberg [8] and Yoshino et al. [9], was assigned to the interaction with the $C'^3\Pi_u$ state by Lewis et al. [11]. For the (16,0) band, they observed 4.5 pairs of the $R_2(N)+P_2(N+2)$ lines with $N=3$ to 11, and we confirmed 3.5 pairs with $N=5$ to 11. Those extra lines are presented in Table 1a with E. The limited number of

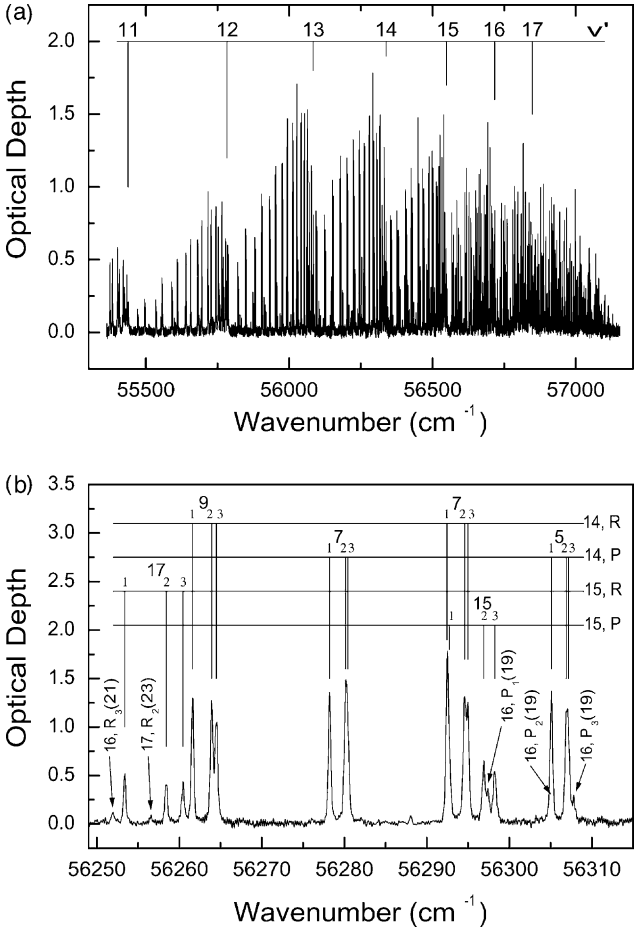

Fig. 1. (a) Absorption cross-section spectrum of the Schumann–Runge bands (55 300–57 400 cm^{-1}) from (12,0) to (17,0) obtained with 4 Torr of oxygen. (b) An expanded portion of the spectrum of the (14,0) band in the region of 56 250–56 310 cm^{-1}.

observations of these weak extra lines is due to the low column density of our absorption measurements. For the (17,0) band, the line at 56448.523 cm^{-1} was assigned to $R_3(19)$, but Lewis et al. [11] designated it as an extra line of $R_2(19)$ without making any assignment to the $R_3(19)$ line. The assignments of the $R_{2,3}$ lines are kept the same as those of Brix and Herzberg [8] and Yoshino et al. [9], and their intensities will be discussed in the following subsection. The extra lines observed for the (17,0) band are also presented in Table 1a with E. The perturbation related with the F_3 level of $v'=16,17$ was also discussed by Lewis et al. [11], but we could not confirm any of those lines in the expected places.

The wavenumber scale in an FT spectrum is strictly linear, and therefore only one reference line is needed to fix the scale absolutely. In previous work we have used as reference the Hg I line at 184.8 nm (having fitted the isotope and hyperfine structure). This line appears in the (8,0) band of the Schumann–Runge system, outside the range of the present measurements, but we have carried the wavenumber calibration through to the

Table 1a
Observed wavenumbers of the principal branch lines of the Schumann–Runge bands of O_2[a]

N	R_1	R_2	R_3	P_1	P_2	P_3
(12,0) band						
1	55784.253	55785.083b		55780.703		
3	55777.781	55778.593b	55778.922b	55769.950	55770.707b	55771.260b
5	55764.225	55765.063b	55765.380b	55751.945	55752.719b	55752.975b
7	55743.605	55744.525b	55744.892b	55726.883	55727.694b	55727.973b
9	55715.943	55716.954b	55717.387b	55694.790	55695.668b	55696.007b
11	55681.214b	55682.348b	55682.846b	55655.627	55656.617b	55657.026b
13	55639.420b	55640.661b	55641.264b	55609.433	55610.540b	55611.017b
15	55590.502	55591.869b	55592.604b	55556.173b	55557.394b	55557.977b
17	55534.482	55536.000b	55536.804b	55495.809	55497.156b	55497.872b
19	55471.235	55472.921b	55473.839b	55428.351	55429.857	55430.643
21	55400.804b	55402.590b	55403.556b			
(13,0) band						
1	56084.434b	56085.701		56081.080		
3	56077.440	56078.674b	56079.008b	56070.131b	56071.324b	56071.898b
5	56063.009	56064.326b	56064.611b	56051.607	56052.800b	56053.06
7	56041.204	56042.622b	56042.979b	56025.667	56026.958b	56027.204b
9	56012.031	56013.576b	56014.051b	55992.373	55993.765b	55994.094b
11	55975.464	55977.15	55977.769	55951.708	55953.239	55953.690
13	55931.497	55933.336	55934.110	55903.672	55905.344	55905.943
15	55880.079	55882.104	55883.036	55848.246	55850.063	55850.820
17	55821.193	55823.391	55824.518	55785.385b	55787.394b	55788.308
19	55754.798	55757.168	55758.519	55715.072	55717.249b	55718.357
21	55680.820b	55683.432b	55684.950	55637.264	55639.613b	55640.946b
23	55599.217	55602.089	55603.795	55551.889	55554.483	55555.982b
25	55509.913	55512.995	55514.907	55458.980	55461.821	55463.433
(14,0) band						
1	56338.537	56340.393		56335.367		
3	56330.945	56332.776b	56333.115b	56324.239	56326.017b	56326.614b
5	56315.553	56317.51	56317.806b	56305.110b	56306.901b	56307.167b
7	56292.443b	56294.571b	56294.960b	56278.209	56280.144b	56280.400b
9	56261.606	56263.928b	56264.492b	56243.609	56245.715b	56246.076b
11	56223.033	56225.572	56226.332	56201.296	56203.590	56204.131
13	56176.682	56179.474b	56180.439	56151.254	56153.764	56154.502b
15	56122.533	56125.569	56126.772	56093.438	56096.217	56097.157b
17	56060.495	56063.845	56065.284	56027.831	56030.849	56032.051
19	55990.537	55994.210b	55995.881	55954.354	55957.669	55959.122
21	55912.606	55916.564	55918.552b	55872.97	55876.618	55878.314
23	55826.598	55830.895	55833.244	55783.675b	55787.615b	55789.564
25	55732.448	55737.195	55739.752	55686.284	55690.561	55692.814
(15,0) band						
1	56547.488	56550.287		56544.549		
3	56539.264b	56542.043b	56542.387b	56533.184b	56535.911	56536.599
5	56522.841	56525.779b	56526.140b	56513.433	56516.168b	56516.440b
7	56498.308	56501.528b	56502.032b	56485.490	56488.416b	56488.734b
9	56465.665	56469.172	56469.911	56449.479b	56452.673b	56453.149b
11	56424.894b	56428.744	56429.757	56405.354	56408.835	56409.550
13	56375.966	56380.168	56381.505	56353.104	56356.936b	56357.928
15	56318.811	56323.419	56325.092b	56292.719b	56296.904	56298.222
17	56253.380	56258.404	56260.451	56224.126	56228.706	56230.343
19	56179.576b	56185.091	56187.525	56147.271	56152.265	56154.290b
21	56097.376b	56103.366	56106.251	56062.091	56067.523	56069.952b
23	56006.557	56013.310b	56016.536	55968.439	55974.405	*55977.284*
25	55907.147	55914.312	55918.320b	55866.272	*55872.988*	55876.161
(16,0) band						
1	56714.654	56718.974	56721.726?	56711.922		
3	56705.765b	56710.046b	56710.497b	56700.350b	56704.601	56705.429b
5	56688.254	56692.735b	56693.248b	56679.929	56684.171b	56684.549b
		56693.671E				
7	56662.217b	56666.791b	56667.797b	56650.912	56655.366b	56655.841b
		56667.595E			56656.332E	

Table 1a (*continued*)

N	R_1	R_2	R_3	P_1	P_2	P_3
9	56627.670	56633.217b	56633.999	56613.384	56617.933	56618.911b
		56632.049E			56618.738E	
11	56584.587	56590.564	56591.800	56567.358	56572.881	56573.639
		56588.623E			56571.713E	
13	56532.932b	56539.377b	56541.112	56512.789	56518.738	56519.969
15	56472.566	56479.625	56481.854	56449.731b	56456.115	56457.820
17	56403.545	56411.163	56414.003	56377.881	56384.909	56387.132
19	56325.680	56333.893	56337.347b	56297.424	56305.009b	56307.839
21	56238.905	56247.667	56251.952	56208.142	56216.360	56219.790
23	56143.083		56157.341	56110.010	56118.764	56123.055
25	56038.115	56047.130		56002.776		56016.962
(17,0) band						
1	56844.985	56851.566		56842.461b		
3	56835.424	56842.048b	56842.585b	56830.693	56837.190b	56838.137
5	56816.843b	56823.719b	56824.240	56809.611	56816.171b	56816.637b
7	56789.311b	56796.591	56797.400	56779.502	56786.351b	56786.833b
9	56752.827	56760.620	56761.876	56740.478	56747.734	56748.519
11	56707.384	56715.719	56717.581b	56692.511b	56700.283b	56701.513
13	56652.945	56661.830	56664.403	56635.591	56643.923	56645.754
15	56589.411	56598.679	56602.206	56569.686	56578.547	56581.094
		56606.869E				
17	56516.705b	56526.050b	56530.835	56494.689	56503.998	56507.454
		56531.874E				
19	56434.713	56443.080	56448.523b	56410.594	56419.940	56424.631b
		56448.523E			56425.705E	
21	56343.320	56356.987b	56361.743	*56317.176*	*56325.525*	*56330.949*
		56349.451E				
23	56242.458	56256.545		56214.398	56228.038	56232.742

b: Incompletely resolved complex.

E: Extra lines resulting from the perturbation.

?: A line is observed at the correct position from the term values, but its intensity is too strong for this assignment. A line might be overlapped with others.

[a] Absolute values of the wavenumbers are subject to the calibration uncertainty of $0.03\,cm^{-1}$. Lines for which the position is affected by an overlapping line or for which the term values are inconsistent are given to two places of decimals only. Values in *italic* are calculated from the combination rule.

Table 1b
Observed wavenumbers of the satellite and forbidden branch lines of the Schumann–Runge bands of O_2

N	${}^{P}R_{13}$	${}^{P}Q_{12}$	${}^{P}Q_{23}$	${}^{R}Q_{21}$	${}^{R}Q_{32}$	${}^{R}P_{31}$	${}^{T}R_{31}$	${}^{N}P_{13}$
(12,0) band								
1	55782.787			55786.960b	55783.552b			
	55782.787	*55778.826*		*55786.960*	*55783.552*	*55785.429*	*55793.091*	
3			55772.768		55776.843			55766.534
	55770.084	*55768.000*	*55772.791*	*55780.543*	*55776.838*	*55778.787*	*55791.193*	*55766.534*
(13,0) band								
1	56083.170	56079.203b		56087.591	56084.190b	56086.066		
	56083.164	*56079.203*		*56087.577*	*56084.190*	*56086.066*	*56093.176*	
3		56068.181	56073.408	56080.643	56076.930			56066.911
	56070.265	*56068.181*	*56073.409*	*56080.624*	*56076.924*	*56078.873*	*56090.423*	*56066.911*
5		56049.624	56054.822					56044.330
	56051.629	*56049.618*	*56054.811*	*56066.314*	*56062.599*	*56064.587*	*56080.362*	*56044.318*
(14,0) band								
1	56337.452b			56342.271	56338.905		56347.316	
	56337.451	*56333.490*		*56342.270*	*56338.905*	*56340.782*	*56347.283*	
3			56328.095					56321.197
	56324.371	*56322.287*	*56328.101*	*56334.725*	*56331.030*	*56332.980*	*56343.619*	*56321.199*
(15,0) band								
1	56546.634			56552.164	56548.881	56550.764	56556.546	
	56546.634	*56542.673*		*56552.164*	*56548.891*	*56550.767*	*56556.556*	

Table 1b (*continued*)

N	$^{P}R_{13}$	$^{P}Q_{12}$	$^{P}Q_{23}$	$^{R}Q_{21}$	$^{R}Q_{32}$	$^{R}P_{31}$	$^{T}R_{31}$	$^{N}P_{13}$
3			56537.996					56530.381
	56533.319	*56531.235*	*56537.996*	*56543.992*	*56540.303*	*56542.253*	*56551.954*	*56530.381*
5								56507.367
	56513.454	*56511.443*	*56518.180*	*56527.773*	*56524.129*	*56526.117*	*56539.417*	*56507.372*
(16,0) band								
1	56714.006			56720.810	56717.721b	56719.598	56724.665b	
	56714.006	*56710.045*		*56720.852*	*56717.721*	*56719.598*	*56724.662*	
3		56698.313	56706.684		56708.412			56697.753
	56700.479	*56698.394*	*56706.684*	*56711.996*	*56708.409*	*56710.359*	*56719.061*	*56697.753*
5		56677.880						56674.731
	56679.953	*56677.941*	*56686.183*	*56694.723*	*56691.237*	*56693.225*	*56705.180*	*56674.531*
(17,0) band								
1	56844.555	56840.417		56853.443	56850.474b	56852.306	56856.758b	
	56844.545	*56840.584*		*56853.443*	*56850.429*	*56852.306*	*56856.753*	
3			56839.367				56850.084b	56828.302
	56830.822	*56828.738*	*56839.274*	*56844.000*	*56840.500*	*56842.450*	*56850.052*	*56828.292*
5							56834.829b	56804.875b
	56809.623	*56807.612*	*56818.187*	*56825.708*	*56822.228*	*56824.216*	*56834.787*	*56804.875*
7								56772.257
	56779.459	*56777.486*	*56788.325*	*56798.607*	*56795.430*	*56797.446*	*56810.802*	*56772.216*
9								56730.577
	56740.384	*56738.438*	*56749.679*	*56762.660*	*56759.929*	*56761.969*	*56778.034*	*56730.574*

Absolute values of the wavenumbers are subject to the calibration uncertainty of $0.03\,cm^{-1}$. Values in *italic* are calculated from the term values. b: Incompletely resolved complex.

(13,0) band by using lines from another of our recorded spectra that overlaps both bands. This step-by-step calibration is a well-known technique. Its accuracy in this case is limited by the large widths of the rotational lines in the (8,0) band (1.5–2.0 cm^{-1} FWHM) [35] that are used for the transfer, which make it difficult to deconvolute their fine structure splitting accurately. The uncertainty in the absolute wavenumber derived in this way is estimated to be $0.03\,cm^{-1}$. However, uncertainties of the relative positions for the strong unblended P_1 and R_1 lines are better than $0.01\,cm^{-1}$. Fig. 2 shows the differences in the observed line positions between the results of the present FT spectroscopic measurement and the previous measurements of Yoshino et al. [9]. The positions of the unblended strong lines are in good agreement of $< 0.1\,cm^{-1}$. The differences are larger for some F_2 and F_3 lines because of insufficient resolution for these blended lines in the previous measurements, and they are also larger for the weak lines, where the discrepancies may be due to the uncertainties arising from the lower S/N ratios in the FT spectra.

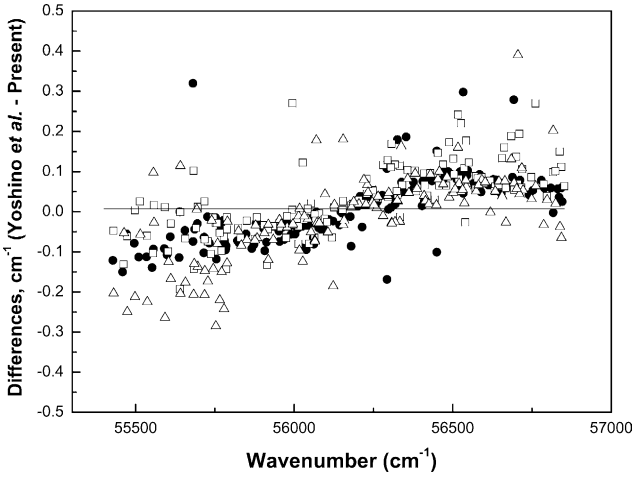

Fig. 2. Differences in the observed line positions between present results and Yosino et al. [9]. The differences of P_1 and R_1 lines are presented by solid circles, P_2, R_2 and P_3, R_3 are presented by open squares and open triangles, respectively. The solid horizontal line represents the average shift of $0.007\,cm^{-1}$.

The rotational term values of the $B(v)$ levels can be obtained by adding the term values of the $X(0)$ level to the wavenumbers of the observed lines. The rotational term values of the ground state for each of three sublevels designated F_1, F_2, and F_3 were provided by Amiot and Verges [36]. The energy origin of these term values is taken for the hypothetical level F_2, $N = J = 0$ of the $X(0)$ level. The rotational term values of the levels with $v = 12$ to 17 obtained in the present work are listed in Table 2 with the estimated uncertainty of the average in 1σ limits. The term values obtained from the extra lines for the $v = 16$ and 17 levels are also shown in *italic* in Table 2. The uncertainties in the term values of high J levels increases because of the decreasing S/N ratios for the lines. For the levels with $v = 16$ and 17, the blended lines in the band head region have influence on the uncertainties of the term values. Note that the *absolute* values of all terms have a possible systematic error of up to $0.03\,cm^{-1}$ arising from the uncertainty in the calibration.

Table 2
The term values of the $B^3\Sigma_u^-$ state of O_2[a]

N	$v=12$			$v=13$		
	F_1	F_2	F_3	F_1	F_2	F_3
0	55781.701(5)			56082.078(2)		
2	55785.252(6)	55787.958(50)	55786.427(5)	56085.432(4)	56088.576(5)	56087.065(22)
4	55793.083(10)	55795.845(18)	55794.089(13)	56092.744(3)	56095.926(3)	56094.175(8)
6	55805.365(8)	55808.189(9)	55806.495(2)	56104.146(6)	56107.452(3)	56105.725(3)
8	55822.094(19)	55825.020(6)	55823.413(12)	56119.684(5)	56123.117(14)	56121.500(10)
10	55843.254(3)	55846.306(12)	55844.794(3)	56139.340(4)	56142.928(4)	56141.458(10)
12	55868.843(10)	55872.037(7)	55870.614(21)	56163.090(7)	56166.841(4)	56165.539(2)
14	55898.836(21)	55902.158(5)	55900.861(12)	56190.910(3)	56194.830(4)	56193.705(8)
16	55933.165(13)	55936.633(5)	55935.488(17)	56222.741(2)	56226.869(2)	56225.922(2)
18	55971.835(13)	55975.476(2)	55974.420(8)	56258.550(5)	56262.868(6)	56262.134(19)
20	56014.715(49)	56018.540(3)	56017.616(34)	56298.279(14)	56302.787(31)	56302.296(62)
22	56061.820	56065.764	56064.906	56341.837(11)	56346.607(14)	56346.300(51)
24			56389.199(76)	56394.229(66)	56394.102(51)	
26			56440.165	56445.440	56445.564	
	$v=14$			$v=15$		
0	56336.366(8)		56545.548(11)			
2	56339.538(6)	56343.268(7)	56341.781(29)	56548.486(5)	56553.163(10)	56551.766(14)
4	56346.247(7)	56350.027(4)	56348.282(2)	56554.569(4)	56559.294(6)	56557.555(7)
6	56356.690(9)	56360.639(7)	56358.921(9)	56563.971(13)	56568.911(19)	56567.255(14)
8	56370.923(5)	56375.067(6)	56373.482(7)	56576.791(7)	56582.025(13)	56580.555(8)
10	56388.921(6)	56393.280(7)	56391.898(7)	56592.980(4)	56598.524(4)	56597.318(6)
12	56410.665(6)	56415.261(3)	56414.099(8)	56612.520(11)	56618.434(5)	56617.525(4)
14	56436.099(5)	56440.985(32)	56440.038(4)	56635.381(6)	56641.666(6)	56641.104(11)
16	56465.192(15)	56470.330(11)	56469.661(14)	56661.478(6)	56668.183(11)	56667.968(16)
18	56497.843(13)	56503.304(20)	56502.899(10)	56690.743(10)	56697.882(10)	56698.067(5)
20	56534.003(16)	56539.799(53)	56539.661(7)	56723.069(54)	56730.704(13)	56731.302(13)
22	56573.623(15)	56579.738(18)	56579.892(45)	56758.392(9)	56766.535(26)	56767.602(26)
24	56616.541(12)	56623.015(29)	56623.517(75)	56796.511(18)	56805.434(94)	56806.854(49)
26	56662.700	56669.641	56670.409	56837.399(18)	56846.758(23)	56848.978(00)
	$v=16$			$v=17$		
0	56712.920(14)		56843.459(37)			
2	56715.646(22)	56721.851(20)	56720.597(8)	56845.989(14)	56854.442(33)	56853.304(6)
4	56721.067(18)	56727.297(11)	56725.661(12)	56850.738(20)	56859.302(11)	56857.752(15)
6	56729.392(15)	56735.861(21)	56734.363(14)	56857.981(24)	56866.846(30)	56865.354(1)
		56736.812(18)				
8	56740.693(11)	56747.291(18)	56746.318(11)	56867.790(7)	56877.086(18)	56875.925(8)
		56748.090(30)				
10	56754.984(10)	56762.574(17)	56761.409(10)	56880.139(26)	56889.972(27)	56889.281(14)
		56761.406(19)				
12	56772.215(15)	56780.247(16)	56779.566(6)	56895.009(16)	56905.414(14)	56905.346(14)
		56778.313(10)				
14	56792.393(40)	56800.879(14)	56800.704(5)	56912.354(20)	56923.318(16)	56923.989(17)
16	56815.233(15)	56824.387(8)	56824.743(8)	56932.059(18)	56943.459(28)	56945.080(18)
					56951.633(18)	
18	56840.903(6)	56850.633(16)	56851.617(16)	56954.074(11)	56965.551(20)	56968.408(37)
					56971.330(9)	
20	56869.159(24)	56879.523(21)	56881.142(37)	56978.193(10)	56988.699(8)	56992.300(35)
22	56899.939(29)	56910.865(28)	56913.338(53)	57004.341(16)	57020.161(29)	57023.085(26)
					57012.625(78)	
24	56933.030(13)	56947.650(45)	57032.406(24)	57048.668(14)		
26	56968.366(20)	56979.575(60)				

[a] Absolute values of the wavenumbers are subject to the calibration uncertainty of $0.03\,cm^{-1}$. Errors of 1σ limits are given in the parentheses. The term values without errors were determined by only one observed line. Italic figures are the term values from the extra lines.

The molecular constants of the $B^3\Sigma_u^-$ state of O_2 from $v=1$ to 17 were derived by Cheung et al. [10] from the experimental data of Yoshino et al. [9]. They performed nonlinear least-square fitting for the matrix elements of the Hamiltonian for a $^3\Sigma$ electronic state in Hund case (a) basis, and determined the band origin T_v; the rotational parameters B_v (rotational coefficient) and D_v (rotational distortion coefficient); λ (spin–rotational

interaction coefficient) and λ_D (coefficient of the rotational distortion for the spin–rotational interaction); γ (spin–spin interaction coefficient) and γ_D (coefficient of the rotational distortion for the spin–spin interaction). We performed the same fitting analysis with the present new term values, except for $F_2(8)$ and $F_2(10)$ of the $v = 16$ level and $F_2(N)$, $N \geqslant 16$ and $F_3(N)$, $N \geqslant 18$ of the $v = 17$ level, because these rotational levels are perturbed as mentioned before. Fig. 3 shows the differences between measured and calculated term values for $v = 14$ and 16. The two values are in good agreement for $v = 14$. Even for the high rotational levels, which have large error bars because of the weak line intensities, the discrepancies are less than $0.07\,\mathrm{cm}^{-1}$, and this is true for all of the term values of $v = 12$ to 15. On the other hand, shifts in the term values are observed around $N = 8$ of the $v = 16$ level, as shown in Fig. 3. A large shifts in the F_2 and F_3 components of the $v = 17$ level are also observed above $N = 16$. The shifts of the F_2 component due to the perturbation with $C'^3\Pi_u$ level occur between $N = 18$ and $N = 20$ [11]. The reason for the shifts of the F_3 component are not clear at present. For the $v = 17$ level, we did not present values of λ_D and γ_D, because the high rotational levels are not used in the least-square fitting. The molecular constants obtained in the present analysis are shown in Table 3, together with the values of Cheung et al. [10].

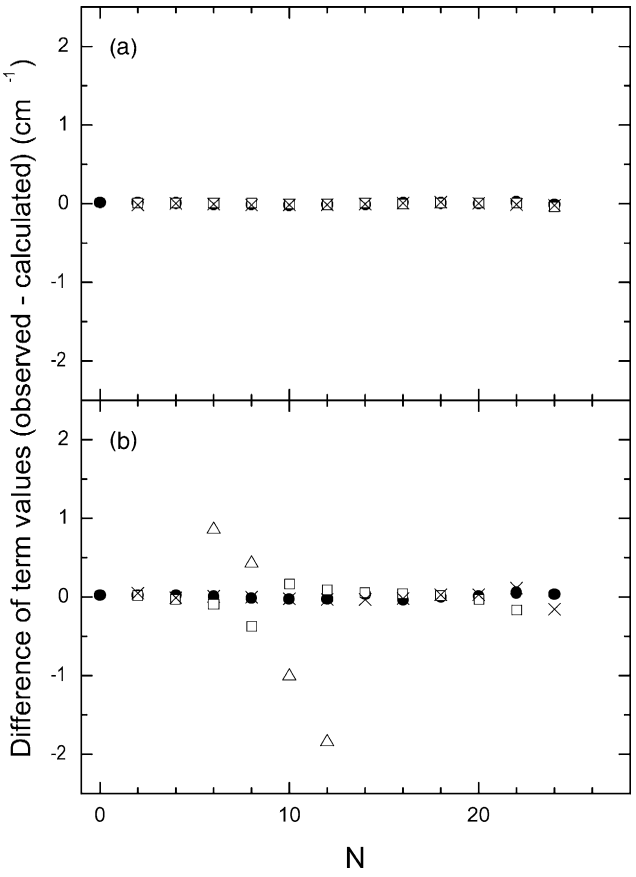

Fig. 3. Differences between measured rotational term values and calculated term values for the $v' = 14$ (a) and $v' = 16$ (b). The differences of T_1, T_2, and T_3 are presented by solid circles, open squares, and crosses, respectively.

3.3. The integrated cross-sections of the lines and band oscillator strengths

The integrated optical depth of each rotational line is obtained along with the line position by the Voigt fitting procedure and is converted to an integrated cross-section by dividing by the column densities given in Section 2. The results are presented in Tables 4a and 4b for the six principal branches and for the satellite and forbidden branches, respectively. For the (13,0)–(15,0) bands, the

Table 3
Molecular spectroscopic constants (cm^{-1}) of the $B^3\Sigma_u^-$ state $v = 12$ to 17 of O_2.[a]

v	$T(v)$[b]	B	10^5D	λ	$-\gamma$	$10^3\lambda_D$	$-10^4\gamma_D$	RMS[c]
12	55783.011(7)	0.56283(9)	1.42(2)	2.24(1)	0.0632(9)	0.24(5)	0.09(3)	0.02
	55782.95(2)	*0.5626(2)*	*1.37(2)*	*2.37(2)*	*0.054(2)*		*0.24(4)*	
13	56083.695(3)	0.52436(3)	1.635(7)	2.488(4)	0.0848(4)	0.02(2)	0.21(1)	0.03
	56083.68(1)	*0.5242(1)*	*1.63(1)*	*2.51(1)*	*0.084(1)*		*0.26(2)*	
14	56338.380(4)	0.48320(4)	2.041(8)	2.793(5)	0.1174(5)	0.24(3)	0.35(1)	0.02
	56338.43(1)	*0.48319(8)*	*2.084(9)*	*2.81(2)*	*0.116(1)*	*0.19(4)*	*0.39(2)*	
15	56548.168(5)	0.43885(5)	2.42(1)	3.269(6)	0.1672(6)	0.40(3)	0.60(2)	0.04
	56548.26(1)	*0.4391(1)*	*2.54(2)*	*3.30(2)*	*0.164(2)*	*0.31(7)*	*0.66(4)*	
16	56716.53(2)	0.3931(2)	2.98(3)	4.05(2)	0.242(2)	0.58(11)	0.80(6)	0.06
	56716.64(2)	*0.3934(2)*	*3.08(3)*	*4.11(3)*	*0.241(3)*	*0.33(1)*	*0.81(6)*	
17	56848.56(2)	0.3463(2)	3.70(5)	5.14(2)	0.352(2)			0.05
	56848.65(4)	*0.3457(8)*	*3.34(31)*	*5.18(3)*	*0.348(3)*			

[a] Estimated errors, which are 1σ limits, are given in parentheses following the last figure of the molecular parameters. Italic parameters below the present results are determined by the previous work of Cheung et al. [10].

[b] Absolute values of $T(v)$ are subject to the calibration uncertainty of $0.03\,\mathrm{cm}^{-1}$.

[c] RMS is the root-mean-square deviation between calculated and observed term values.

Table 4a
Integrated cross-sections of the main branch lines of the Schumann–Runge bands of O_2 in units of $10^{-19}\,cm^2\,cm^{-1}$ [a]

N	R_1	R_2	R_3	P_1	P_2	P_3	R_1	R_2	R_3	P_1	P_2	P_3
	(12,0) band						(13,0) band					
1	2.90	1.67b		2.14			3.17b	1.74		2.03		
3	4.77	3.82b	2.89b	4.25	2.27b	1.54b	4.85	4.22b	2.46b	5.04b	2.68b	1.54b
5	6.02	5.03b	3.89b	5.17	4.20b	2.97b	5.89	5.31b	4.52b	5.11	4.31b	3.49
7	6.24	5.52b	4.83b	5.41	4.68b	4.29b	5.91	5.55b	5.29b	5.44	5.39b	4.54b
9	5.71	5.25b	4.53b	5.58	4.76b	4.24b	5.93	5.00b	5.12b	5.30	5.46b	4.55b
11	5.20b	4.32b	3.82b	4.68	4.46b	4.14b	5.10	5.74	4.30	4.90	4.80	3.89
13	4.19b	3.81b	3.25b	3.55	3.71b	3.33b	3.91	3.94	4.02	4.10	3.91	3.79
15	2.82	2.67b	2.48b	2.53b	2.66b	2.55b	3.37	3.03	2.93	3.28	3.37	2.58
17	2.10	1.68b	1.68b	1.95	1.83b	1.78b	2.07	2.45	2.13	2.43b	2.53b	2.05
19	1.19	1.57b	1.08b	1.42	0.88	0.80	1.80	1.46	1.61	1.45	1.78b	1.34
21	0.89b	0.61b	0.75b				0.72b	1.26b	0.85	0.76	0.89b	0.53b
23							0.42	0.33	0.45	0.27	0.44	0.67b
25							0.16	0.13	0.30	0.29	0.30	0.24
Total	42.03	35.95	29.19	36.69	29.46	25.64	43.30	40.14	34.00	40.40	35.87	29.22
Ext.	42.62	36.65	29.91	37.89	31.12	27.56	43.45	40.41	34.30	40.59	36.26	29.56
	(14,0) band						(15,0) band					
1	3.08	2.05		2.47			3.06	1.68		1.99		
3	5.76	4.16b	2.94b	4.24	2.99b	1.49b	4.35b	3.77b	3.46b	3.90b	2.95	1.52
5	6.13	6.16	4.91b	4.80b	4.86b	3.82b	5.91	5.28b	4.02b	5.49	4.72b	3.25b
7	6.26b	6.31b	5.16b	5.85	5.44b	4.84b	6.20	6.15b	4.98b	6.41	5.57b	4.58b
9	6.04	6.41b	5.37b	5.86	5.63b	5.20b	5.94	5.59	5.36	6.62b	5.86b	4.84b
11	4.93	5.33	4.36	4.88	4.88	4.64	5.87b	4.92	4.56	5.01	4.55	4.81
13	4.18	3.94b	3.80	4.25	3.88	3.99b	4.16	4.05	3.53	3.83	4.83b	3.34
15	3.03	2.97	2.80	3.26	2.96	2.81b	2.97	2.97	2.89b	3.55b	3.02	3.36
17	2.23	2.28	1.73	2.13	2.06	1.92	2.41	2.27	2.43	2.42	2.36	2.80
19	1.55	1.36b	1.62	1.78	1.42	1.41	1.37b	1.42	1.37	1.21	1.57	1.35b
21	0.77	0.72	0.56b	1.44	1.01	0.87	0.66b	0.73	1.00	1.28	0.79	0.38b
23	0.59	0.66	0.36	0.39b	0.45b	0.79	0.48	0.74b	0.81	0.60	0.54	
25	0.57	0.33	0.33	0.25	0.23	0.13	0.22	0.14	0.16b	0.16		0.35
Total	45.11	42.69	33.96	41.60	35.82	31.92	43.60	39.72	34.57	42.47	36.66	30.57
Ext.	45.21	42.84	34.16	41.86	36.07	32.32	43.76	39.92	34.88	42.56	37.40	31.72
	(16,0) band						(17,0) band					
1	2.40	2.20	1.08?	1.53			2.39	1.45		1.73b		
3	4.49b	4.43b	3.01b	4.08b	3.27	0.92b	3.47	3.68b	1.65b	3.17	2.26b	0.91
5	5.45	4.91b	4.16b	5.26	4.25b	3.08b	4.44b	5.09b	4.94	3.98	4.13b	2.77b
		0.39										
7	5.22b	2.14	4.11b	5.26	4.76b	3.67b	3.94b	4.98	3.86	4.66	4.85b	2.98b
		2.80			*0.75*							
9	5.28	4.28	4.67	5.30	2.54	4.59b	4.69	4.67	3.74	6.83	6.07	2.94
		1.03			*2.65*							
11	4.58	4.07	4.43	4.43	3.76	3.81	3.83	4.08	4.00b	3.52b	3.24b	3.12
		0.21			*0.59*							
13	4.33b	3.73b	4.01	4.98	3.51	3.40	3.17	3.29	2.80	2.99	2.86	2.55
15	2.57	2.43	2.25	2.42b	2.52	2.39	2.14	2.94	2.49	2.30	2.24	2.19
								0.20				
17	1.63	1.72	1.69	1.76	1.75	1.70	1.53b	1.84b	1.44	1.44	2.04	1.59
								0.19				
19	1.51	1.20	0.99b	1.18	1.39b	0.92	0.90	0.45	0.98	0.90	0.74	0.72b
											0.17	
21	0.81	0.86	0.79	0.81	0.85	0.81	0.76	0.68b	0.49			
								0.12				
23	0.34		0.30	0.31	0.28	0.22	0.52	0.32		0.62	0.39	0.48
25	0.16	0.08		0.26		0.11						
Total	38.77	36.48	30.42	37.58	32.87	25.62	31.78	33.98	26.39	32.12	29.00	20.24
Ext.	38.90	36.88	30.76	37.70	33.25	25.90	32.03	34.22	27.33	32.97	29.95	21.57

b: Incompletely resolved complex.
[a] Extra lines resulting from the perturbation presented in *italic*.

Table 4b
Integrated cross-sections of the satellite and forbidden branch lines of the Schumann–Runge bands of O_2 in units of $10^{-19}\,cm^2\,cm^{-1}$

Band	N	${}^{P}R_{13}$	${}^{P}Q_{12}$	${}^{P}Q_{23}$	${}^{R}Q_{21}$	${}^{R}Q_{32}$	${}^{R}P_{31}$	${}^{T}R_{31}$	${}^{N}P_{13}$
(12,0)	1	1.01			0.44b	1.39b			
	3			0.59		0.51			0.71
	Total	1.01		0.59	0.44	1.90			0.71
(13,0)	1	1.03	0.39b		0.60	1.65b	0.08		
	3		0.24	0.44	0.13	0.41			0.57
	5		0.14	0.52					0.74
	Total	1.03	0.77	0.96	0.73	2.06	0.08		1.31
(14,0)	1	1.92b			0.98	1.91		0.05	
	3			0.92					0.73
	Total	1.92		0.92	0.98	1.91		0.05	0.73
(15,0)	1	1.11			0.98	1.57	0.39	0.31	
	3			0.54					0.42
	5								0.53
	Total	1.11		0.54	0.98	1.57	0.39	0.31	0.95
(16,0)	1	1.46				0.75b	0.42	0.58b	
	3		0.25	0.74		0.53			0.91
	5		0.61						1.99
	Total	1.46	0.86	0.74		1.28	0.42	0.58	2.90
(17,0)	1	0.84	0.69		0.39	2.34b	1.17	0.46b	
	3							1.21b	1.02
	5							0.62b	0.70b
	7								1.26
	9								0.34
	Total	0.84	0.69		0.39	2.34	1.17	2.28	3.32

b: Incompletely resolved complex.

present results were determined from the measurements with 2.00 Torr pressure of oxygen. The integrated cross-sections of the strong lines ($N = 7$ to 13) obtained from the measurements with 4.00 Torr of oxygen are systematically lower than those at 2.00 Torr. These lines are very narrow, and it is possible that our resolution is not high enough to avoid errors from saturation. Therefore the cross-sections from the 4.00 Torr pressure were not included in the present results. The spectrum at 10 Torr pressure was not used at all for the integrated cross-sections because of intensity saturation. The integrated cross-sections of the R_1, R_2, and R_3 branch lines of the (14,0) band are plotted against N in Fig. 4a, represented by the solid squares, circles, and triangles, respectively. The values listed in Tables 4a and 4b can be divided by the fractional populations of the rotational levels to obtain values proportional to the line oscillator strengths.

The extra lines observed in the (16,0) and (17,0) bands are results of the heterogeneous perturbation between $B^3\Sigma_u^-$ and $C'^3\Pi_u$ states discussed by Lewis et al. [11]. The almost equal intensities observed for the main and extra $P_2(9)$ and $R_2(7)$ lines of the (16,0) band results from the maximum interaction at the $v' = 8$ level as shown in Fig. 4 of [11]. The strengths of the extra lines are borrowed from the perturbed levels of the $B^3\Sigma_u^-$ state. The results of the perturbation on their intensity are demonstrated in Fig. 4b for the P_2 branch of the (16,0) band. The sum of the integrated cross-sections of the main and extra lines is used for the total and extended values, because the band oscillator strength of the $C'^3\Pi_u$–$X^3\Sigma_g^-$ system is negligible compared to that of the S–R band system. As mentioned in the previous section for the (17,0) band, Lewis et al. [11] reassigned a line at $56448.523\,cm^{-1}$ from $R_3(19)$ to an extra line of $R_2(19)$. However, then the total strength of $R_2(19)$ line (the main and extra) will be $1.43 \times 10^{-19}\,cm^2\,cm^{-1}$, which is too large compared with that of the $R_1(19)$ line. On the other hand, the strength of $R_2(19)$ is too weak by itself. Therefore we propose that the line at $56448.523\,cm^{-1}$ is a blend of two lines, $R_3(19)$ and the extra line of $R_2(19)$.

The strengths of the branches are obtained by adding the integrated cross-sections of all rotational lines in the branch. These are listed in Tables 4a and 4b as 'Total.' The high rotational lines of $N > 25$ are not observed in the present measurements because they are too weak with respect to the photon noise level. However, these higher N lines should be taken into account for the total branch cross-sections. The extended total cross-section of each branch up to $N'' = 41$ was obtained by the extrapolation method using the Boltzmann distribution as

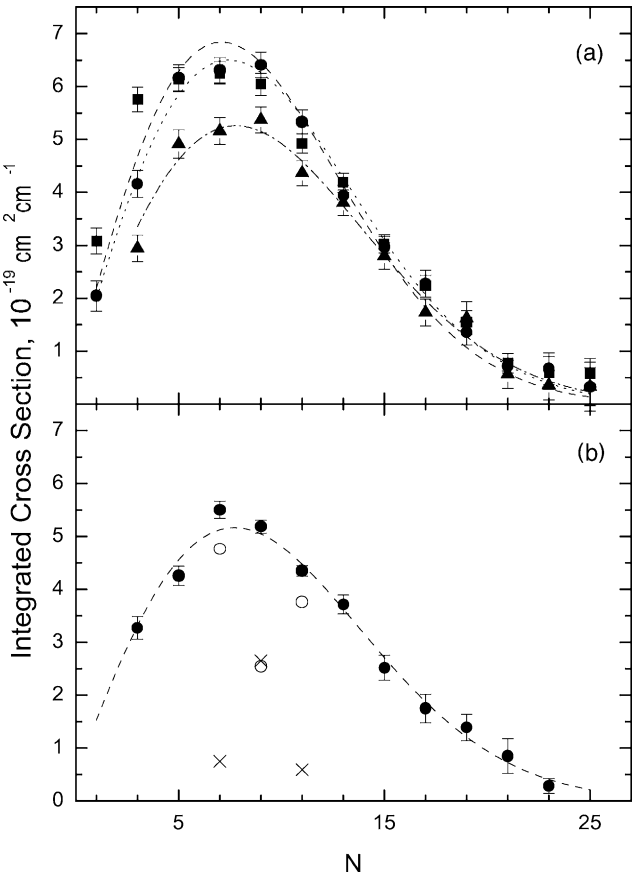

Fig. 4. (a) The integrated cross-sections of the R_1, R_2, and R_3 branch lines of (14,0) band against N. The results of the measurements are shown by solid squares, circles, and triangles, respectively. Fitted curves of the Boltzmann distribution are shown by broken, dotted, and chain lines, respectively. (b) The integrated cross-sections of the P_2 branch lines of (16,0) band. The total, main, and extra lines are shown by solid circles, open circles, and crosses, respectively.

discussed by Yoshino et al. [28], and it is given in the bottom line in Table 4a. The total integrated cross-sections of the satellite and the forbidden branches were not extended because the fractional intensity distribution of these branches decreases rapidly with J. Table 5 gives the total observed integrated cross-section for each band, obtained by summing over all branches, together with the total extended integrated cross-section obtained by using the extended integrated cross-sections for the principal branches.

The uncertainties in the integrated cross-sections are due to noise in the spectra and errors in the measurement of the O_2 pressure and optical path length. The small errors in the pressure (± 0.02 Torr), temperature (295 ± 2 K), and path length (7.82 ± 0.01 cm) give a random error of less than 2%. The error from the noise of the background is almost constant at $\pm 3 \times 10^{-20}$ cm^2 over the whole spectrum. For the unblended strong lines of $5\text{–}6 \times 10^{-19}$ cm^2 cm^{-1}, the uncertainties due to noise are estimated to be 3–4%. For weak lines of integrated cross-section 2.5×10^{-19} cm^2 cm^{-1} the uncertainty is 10%, and for 1.0×10^{-19} cm^2 cm^{-1} it is 17%. The large uncertainties of the weak peaks do not significantly affect the integrated cross-sections of the bands because these are determined predominantly by the strong lines. Therefore, total errors on the integrated cross-sections are estimated to be less than 5%.

The band oscillator strength of the (v', v'') band is given by

$$f(v', v'') = \frac{mc^2}{\pi e^2} \frac{1}{\tilde{N}(v'')} \int \sigma(v)\,dv \tag{1}$$

in which $\tilde{N}(v'')$ is the fractional Boltzmann population of the absorbing vibrational level, and integration of the cross-section $\sigma(v)$ is performed over all of the rotational lines belonging to the (v', v'') band. Table 5 shows the oscillator strengths of the bands $v' = 12$ to 17 obtained in the present work from the extended total cross-sections of principal branches and the observed total cross-sections of satellite and forbidden branches. Table 5 also shows the results obtained in earlier measurements. The

Table 5
Total and extended integrated cross-sections (10^{-17} cm^2 cm^{-1}), and band oscillator strengths (10^{-5}) of the Schumann–Runge bands of O_2

Band	Integrated cross-sections		Band oscillator strengths, f					
	Total[a]	Ext.[b]	Present	LBC[c]	YFEP[d]	GGMBL[e]	HCMK[f]	Bethke[g]
(12,0)	2.04	2.10	2.38	2.44	2.43	2.74	2.88	2.81
(13,0)	2.30	2.32	2.62	2.73		2.87	3.41	3.17
(14,0)	2.38	2.39	2.70	2.82		3.21	3.77	3.24
(15,0)	2.33	2.36	2.66	2.73		2.95	3.73	3.26
(16,0)	2.10	2.12	2.40	2.63		2.63	3.53	3.16
(17,0)	1.83	1.88	2.12			2.64	3.03	2.95

[a] Total integrated cross-sections from Tables 4a and 4b.
[b] Extended integrated cross-sections from Tables 4a and 4b.
[c] LBC: Lewis et al. [20].
[d] YFEP: Yoshino et al. [21].
[e] GGMBL: Gies et al. [19].
[f] HCMK: Huebner et al. [14].
[g] Bethke [13].

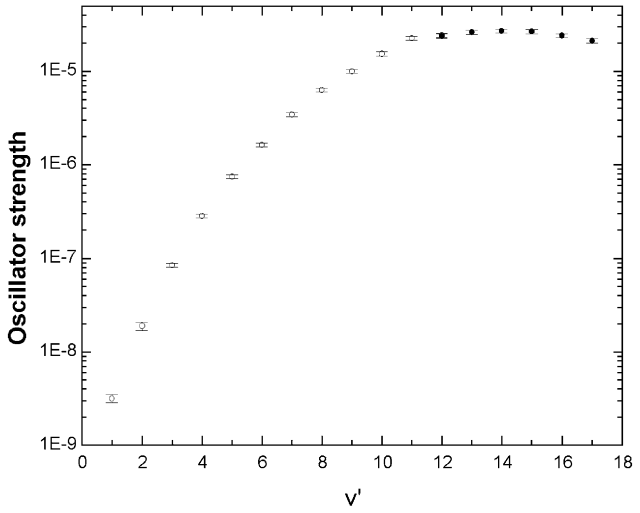

Fig. 5. Band oscillator strengths with $v' = 1$ to 17. The oscillator strengths of $v' = 1$ to 12 derived from the measurement of Yoshino et al. [21] are shown in the open circles. Present results of $v' = 12$ to 17 are marked by solid circles.

present band oscillator strength of the (12,0) band agrees with the result of Yoshino et al. [21] obtained by line-by-line photoabsorption cross-section measurement with a resolution of $0.40\,\mathrm{cm}^{-1}$. The oscillator strengths of the present work are smaller than those of Bethke [13] and Gies et al. [19] and much smaller than that of Huebner [14] obtained by electron energy loss measurement. The results of Lewis et al. [20], obtained by measurement without pressure broadening with a resolution of $1.4\,\mathrm{cm}^{-1}$ are near the present results, but still a little larger. Our value is the only one derived from line-by-line measurements with a resolution comparable to the rotational linewidths for the bands of $v' \geqslant 13$. Moreover, we were able to separate the lines of one vibrational band from those of overlapping higher vibrational bands. Because this could not be done in the previous (low resolution) measurements, it is possible that the blending may have led to overestimates of the band oscillator strengths by those authors. Fig. 5 shows a plot of band oscillator strengths against v' for $v' = 1$ to 17, using the results of the present work and those of Yoshino et al. [21].

4. Summary

This work provides the first absorption measurements of the Schumann–Runge (13,0)–(17,0) bands of O_2 free of problems arising from inadequate spectral resolution. In addition, this is the first measurements of the Schumann–Runge bands performed by the combination of a VUV FT spectrometer and a synchrotron radiation source. The present measurements provide accurate rotational line positions, term values and oscillator strengths of the (12.0)–(17,0) bands.

Acknowledgments

This work was supported in part by a NSF Division of Atmospheric Sciences Grant No. ATM-91-16552 to Harvard College Observatory, and by the NASA Upper Atmospheric Research Program under Grant No. NAG5-484 to the Smithsonian Astrophysical Observatory. We also acknowledge the Paul Instrument Fund of the Royal Society for the development of the VUV-FT spectrometer. We thank Dr. Lewis for sending the unpublished term values of the F_3 levels of the B(16) and B(17) levels. The FT spectroscopic measurements at the Photon Factory were made with the approval of the Photon Factory Advisory Committee (94G367). K.Y. thanks the Japan Society for the Promotion of Science for support. A.P.T. thanks NATO for support from a Grant for International Collaboration in Research (#890224).

References

[1] P.S. Julienne, M. Krauss, J. Mol. Spectrosc. 56 (1975) 270–308.
[2] M. Nicolet, P. Mange, J. Geophys. Res. 59 (1954) 15–45.
[3] P.E. Krupenie, J. Phys. Chem. Ref. Data 1 (1972) 423–534.
[4] D.M. Creek, R.W. Nicholls, Proc. Roy. Soc. (London) A 341 (1975) 517–536.
[5] K.P. Huber, G. Herzberg, Molecular Spectra and Molecular Structure. IV: Constants of Diatomic Molecules, van Nostrand Reinhold, New York, 1979.
[6] J. Curray, G. Herzberg, Ann. Phys. 19 (1934) 800–808.
[7] H.P. Knauss, S.S. Ballard, Phys. Rev. 48 (1935) 796–799.
[8] P. Brix, G. Herzberg, Can. J. Phys. 32 (1954) 110–135.
[9] K. Yoshino, D.E. Freeman,, W.H. Parkinsom, J. Phys. Chem. Ref. Data 13 (1984) 207–227.
[10] A.S.-C. Cheung, K. Yoshino, W.H. Parkinson, D.E. Freeman, J. Mol. Spectrosc. 119 (1986) 1–10.
[11] B.R. Lewis, P.M. Dooley, J.P. England, K. Waring, S.T. Gibson, K.G.H. Baldwin, Phys. Rev. A 54 (1996) 3923–3938.
[12] K. Waring, B.R. Lewis, K.G.H. Baldwin, S.T. Gibson, J. Chem. Phys. 115 (2001) 5836–5842.
[13] G.W. Bethke, J. Chem. Phys. 31 (1959) 669–673.
[14] R.H. Huebner, R.J. Celotta, S.R. Mielczarek, C.E. Kuyatt, J. Chem. Phys. 63 (1975) 241–247.
[15] J.E. Frederick, R.D. Hudson, J. Mol. Spectrosc. 74 (1979) 247–258.
[16] B.R. Lewis, J.H. Carver, T.I. Hobbs, D.G. McCoy, H.P. Gies, J. Quant. Spectrosc. Radiat. Trans. 20 (1978) 191–203.
[17] B.R. Lewis, J.H. Carver, T.I. Hobbs, D.G. McCoy, H.P. Gies, J. Quant. Spectrosc. Radiat. Trans. 22 (1979) 213–221.
[18] B.R. Lewis, J.H. Carver, T.I. Hobbs, D.G. McCoy, H.P. Gies, J. Quant. Spectrosc. Radiat. Trans. 24 (1980) 365–369.
[19] H.P. Gies, S.T. Gibson, D.G. McCoy, A.J. Blake,, B.R. Lewis, J. Quant. Spectrosc. Radiat. Trans. 26 (1981) 469–481.
[20] B.R. Lewis, L. Berzins, J.H. Carver, J. Quant. Spectrosc. Radiat. Trans. 36 (1986) 209–232.
[21] K. Yoshino, D.E. Freeman, J.R. Esmond, W.H. Parkinson, Planet. Space Sci. 31 (1983) 339–353.
[22] K. Yoshino, J.R. Esmond, A.S.-C. Cheung, D.E. Freeman, W.H. Parkinson, Planet. Space Sci. 40 (1992) 185–192.
[23] K. Yoshino, D.E. Freeman, J.R. Esmond, W.H. Parkinson, Planet. Space Sci. 35 (1987) 1067–1075.

[24] G. Stark, K. Yoshino, P.L. Smith, K. Ito, W.H. Parkinson, Astrophys. J. 369 (1991) 574–580.
[25] A.P. Thorne, C.J. Harris, I. Wynne-Jones, R.C.M. Learner, G. Cox, J. Phys. E 20 (1987) 54–60.
[26] W.H. Parkinson, A.P. Thorne, G. Cox, P.L. Smith, K. Yoshino, SPIE Proc. 2282 (1994) 59–64.
[27] K. Yoshino, J.E. Murray, J.R. Esmond, Y. Sun, W.H. Parkinson, A.P. Thorne, R.C.M. Learner, G. Cox, Can. J. Phys. 72 (1994) 1101–1108.
[28] K. Yoshino, J.R. Esmond, J.E. Murray, W.H. Parkinson, A.P. Thorne, R.C.M. Learner, G. Cox, J. Chem. Phys. 103 (1995) 1243–1249.
[29] K. Yoshino, J.R. Esmond, W.H. Parkinson, A.P. Thorne, J.E. Murray, R.C.M. Learner, G. Cox, A.S.-C. Cheung, K.W.-S. Leung, K. Ito, T. Matsui, T. Imajo, J. Chem. Phys. 109 (1998) 1751–1757.
[30] K. Ito, T. Namioka, Y. Morioka, T. Sasaki, H. Noda, K. Goto, T. Katayama, M. Koike, Appl. Opt. 25 (1986) 837–847.
[31] K. Ito, T. Sasaki, T. Namioka, K. Ueda, Y. Morioka, Nucl. Instr. Meth. A 246 (1986) 290–293.
[32] J.W. Brault, private communications.
[33] J.B. Tatum, J.K.G. Watson, Can. J. Phys. 49 (1971) 2693–2703.
[34] P.M. Dooley, B.R. Lewis, S.T. Gibson, G.H. Baldwin, P.C. Cosby, J.L. Price, R.A. Copeland, T.G. Slanger, K. Yoshino, A.P. Thorne, J.E. Murray, J. Chem. Phys. 109 (1998) 3856–3867.
[35] A.S.-C. Cheung, K. Yoshino, J.R. Esmond, S.S.-L. Chiu, D.E. Freeman, W.H. Parkinson, J. Chem. Phys. 92 (1990) 842–849.
[36] C. Amiot, J. Verges, Can. J. Phys. 59 (1981) 1391–1398.